POLITECNICO DI TORINO
Repository ISTITUZIONALE

Dermis mechanical behaviour after different cell removal treatments

(Article begins on next page)

01 May 2024

Dermis Mechanical Behaviour after Different Cell Removal Treatments

Mara Terzini[a], Cristina Bignardi[b], Carlotta Castagnoli[c], Irene Cambieri[d], Elisabetta M. Zanetti[e]*, Alberto L. Audenino[f]

[a]DIMEAS, Politecnico di Torino, Cso Duca degli Abruzzi, 10129 Torino (ITALY); E-mail: mara.terzini@polito.it

[b]DIMEAS, Politecnico di Torino, Cso Duca degli Abruzzi, 10129 Torino (ITALY); E-mail: cristina.bignardi@polito.it

[c]Skin Bank, AOU Città della Salute e della Scienza, Via Zuretti 29, 10126 Torino (ITALY); E-mail: ccastagnoli@cittadellasalute.to.it

[d]Skin Bank, AOU Città della Salute e della Scienza, Via Zuretti 29, 10126 Torino (ITALY); E-mail: icambieri@cittadellasalute.to.it

[e]DI, University of Perugia, Via Duranti 67, 06125 Perugia (ITALY); E-mail: elisabetta.zanetti@unipg.it

[f]DIMEAS, Politecnico di Torino, Cso Duca degli Abruzzi, 10129 Torino (ITALY); E-mail: alberto.audenino@polito.it

Running Head: Dermis Mechanical Behavior for Different Cell Removal Treatments

*Contact Author:

Elisabetta M. Zanetti

Department of Engineering

Via Duranti, 67

06125 Perugia (ITALY)

E-mail: elisabetta.zanetti@unipg.it

30 **Abstract**

31 Human acellular dermal matrices (HADMs) are used in reconstructive surgery as scaffolds

32 promoting autologous tissue regeneration. Critical to the HADM ability to remodel and integrate

33 into the host tissue is the removal of cells while maintaining an intact extracellular architecture.

34 The objective of this work is to develop a methodology to analyse the mechanical properties of

35 HADMs after decellularization to identify its ideal form of treatment and its duration.

36 Two different decellularization techniques were used as a benchmark: the first is a well-

37 established technique (incubation in NaOH for 1 to 7 weeks), and the second is an innovative

38 technique developed by this research group (incubation in DMEM (Dulbecco's modified Eagle

39 medium) for 1 to 7 weeks). After decellularization, the specimens underwent uniaxial tensile tests,

40 and experimental data were represented with stress strain curves, calculating both engineering and

41 true values.

42 Mechanical tests have led to the identification of the optimal method (NaOH or DMEM) and

43 duration for the decellularization treatment; differences between engineering and true values can

44 reach 84%, but the engineering values remain useful to make comparisons, providing reliable

45 indications with a simpler experimental set up and data processing.

46

47 *Keywords* – decellularization treatment, human dermis, static mechanical tests, ultimate stress,

48 ultimate strain, Young's modulus

49

1 Introduction

Engineered skin substitutes have a significant medical practice for patients with extensive burn wounds [1]. Advances in tissue engineering suggest that skin substitutes will be indistinguishable from the normal skin in the near future [2]. However, current skin substitutes do not restore the full native skin physiology because they lack some components such as hair follicles, sebaceous glands and sweat glands [2]. Additionally, the engineered tissue cannot faithfully replicate the mechanical properties of the native skin [1].

Currently, alloplastic material and skin allografts, taken from multi-organ donors, are the most suitable integumentary replacement for reconstructive surgery [3]. The immune response to allograft skin is directed primarily against epidermal, endothelial and fibroblast cells in the dermis, while the non-cellular component of the dermis (extracellular matrix) has been demonstrated to be relatively non-immunogenic [4]. Glycerolised acellular alloplastic human dermis (HADM) is used as a matrix for various reconstructive plastic purposes, where it retains almost all of the healthy dermal properties: it is compact and elastic, can be taken into the bed wound, and it retains the intact tissue morphology [5].

Different treatments can be used for tissue decellularization [6]. Commonly, a low concentration of NaOH has been used for this aim. The result of this technique is a reliably decellularized matrix. However, surgeons report that this matrix is inferior with reference to handling, ease of use, elasticity and needle penetration resistance. Additionally, decellularization using sodium hydroxide implies the direct contact of the tissue with an aggressive chemical agent, which must necessarily be neutralized by means of incubation in 0.1 N HCl at the end of the decellularization phase. These are the reasons why, in recent times, our research unit has developed an alternative procedure that aims to overcome these limitations. The new methodology consists of keeping the

3

73   tissue in DMEM (Dulbecco's modified Eagle medium) for a long period of time (several weeks)

74   while being subjected to mechanical action (tilting). From a biological point of view, the

75   efficiency of the different treatments can be verified by means of an immunohistochemistry

76   analysis, but the preservation of the main mechanical properties of the native dermis also needs

77   to be checked [7]. The aim of this work is to evaluate the mechanical properties of tissue subjected

78   to decellularization treatments varying by type and length to establish the best compromise

79   between a reliably complete decellularization and adequate mechanical properties. The

80   mechanical properties here analysed are the elastic modulus and the ultimate load and strain [8],

81   considering that repaired full-thickness burn wounds may be subject to loss due to dermal

82   substitute deficiencies in tensile strength and elasticity [1] and the requirements of soft-tissue

83   augmentation procedures like rotator cuff [9].

84   The skin is made of three layers, the epidermis, dermis, and hypodermis. It consists of collagen

85   (approximately 75% of the dry weight) and elastin (4% of the dry weight) fibres embedded in a

86   gel-like ground substance consisting of water, small solutes, and macromolecules, predominantly

87   proteoglycans [10]. The dermis provides a major contribution to the overall mechanical

88   characteristics of the skin due to its main constituents, collagen and elastin fibrils, which allow

89   high levels of deformation and flexibility as the fibrils stretch and re-orientate [11]. Collagen

90   fibres are crimped and almost inactive at low strains, while they play a major role at high

91   deformations (where they are stiffer than elastin by approximately three order of magnitude [8]).

92   The skin is anisotropic due to the variable orientation of collagen fibres, with a prevalence along

93   the orientation of the so-called Langer's lines [8]. The dermis can therefore be described as an

94   anisotropic, viscoelastic, nonlinear [12] and non-homogenous material.

4

95 The tensile test is the most widely used mechanical test performed on *ex vivo* skin specimens.

96 Using this method, the anisotropic, non-linear and viscoelastic behaviours of skin have been

97 explored, as well as its failure properties [13], creep [14], fatigue [15] and preconditioning

98 behaviour [16]. This test is here being used to assess changes in the biomechanical behaviour

99 produced by alterations of the skin's structure, similarly to the approach followed by those authors

100 who studied variations in the collagen content [14] or elastin and proteoglycans contents [10].

101 Due to section narrowing taking place during the specimen loading, different formulations of

102 stress in mechanical tests can produce different results: these are the so called 'nominal' or

103 'engineering values'; their respective 'true' values can be obtained from engineering values under

104 specific assumptions such as volume constancy [17,18]. As true values provide the most faithful

105 representation of the material properties, their estimation requires a complex and demanding

106 experimental set up. This work is also an attempt to quantify differences among these expressions

107 and their limits, establishing if they can or cannot be used for tissue characterization and/or to

108 make comparisons among decellularization treatments.

109 ## 2 Materials and methods

110 ### 2.1 Specimens

111 Strips of skin tissue, collected from the backs of human donors, were dissected along the cranio-

112 caudal direction. They were decellularized using two different methods based on incubation in

113 0.06 N NaOH or DMEM for 1 to 7 weeks. Immunohistochemistry has been performed for all

114 treatments to verify the decellularization, according to the following procedure. Biopsy samples

115 were washed in physiological solution, fixed in 4% neutral-buffered formalin and embedded in

116 formalin by routine processing (FFPE). FFPE samples were sectioned at a thickness of 2-3 µm

5

117   for immunohistochemistry reactions, and immunohistochemistry was performed using an

118   automated slide-processing platform (Ventana BenchMarckXT Autostainer, Ventana Medical

119   Systems, Tucson, AZ, USA)." HADMs, preserved at 85% glycerol in a 4°C refrigerator at the

120   Turin Skin Bank (Italy) and unfit for transplantation, were used for these experiments after the

121   approval of the Institutional Ethical Board of A*zienda Ospedaliera Universitaria Città della*

122   *Salute e della Scienza* of Turin, Italy, (approved on January 23rd, 2012 with protocol number

123   0006730), and written informed consent was obtained from all study participants. Before use, the

124   dermis grafts were washed to remove all of the glycerol, dipping them sequentially in three

125   different beakers filled with abundant saline solution 0.9% at +37°C for more than three minutes

126   each, as prescribed by the Euro Skin Bank [19]. The specimens were obtained by cutting out

127   approximately 2x4 mm strips along the cranio-caudal (CC) and medio-lateral (ML) directions

128   using a custom made die cutter; this cutting method avoids generating notches and defects that

129   could bias tests. The resulting specimen sizes were measured by means of photogrammetry before

130   mechanical testing: 4.33±0.57-mm width, 2.21±0.32-mm thickness, 10.10±0.38-mm length

131   (average ± std).

132   On the whole, there were 3–4 specimens (depending on the original strip size and shape) for each

133   combination of decellularization method (NaOH or DMEM), duration (called 'Tx' in the

134   following, where x represents the number of weeks of incubation) and cut orientation (CC or ML),

135   for a total 96 specimens. Intact human skin was used as a control (called 'T0' in the following, as

136   it did not undergo any decellularization treatment).

137   ## 2.2   Photogrammetry set-up

138   Two different photographic set-ups have been developed to measure the specimens. The first was

139   finalized to measure the specimens' size at rest and was made of a full-frame digital camera

6

140   (Canon EOS 5D Mark II) with an autofocus lens for macro photography (Canon EF 100 mm f/2.8

141   Macro USM), a camera stand with two light stands, and a tripod. A second set-up was developed

142   to follow tensile tests; it included the previously described digital camera as well as a second

143   digital single-lens reflex camera (Canon EOS 400D). When the two cameras were triggered, they

144   acquired the frontal and lateral views of the specimen through a remote capture software (DSLR

145   Remote Pro). The width and the thickness of the specimens were measured using the image

146   analysis software ImageJ (National Institutes of Health, Bethesda, Maryland, U.S.) as an average

147   of five different measurements, reaching a 0.01 mm/pixel measurement resolution given a 21.0

148   MP image (5616x3744 pixels).

149   ## 2.3   Mechanical tests

150   Samples were subjected to uniaxial tensile tests along both the cranio-caudal and medio-lateral

151   directions to quantify the influence of the chemical treatment on the skin tissue's biomechanical

152   behaviour. Testing parameters have been set according to the physiological loads, the expected

153   tissue behaviour, and the Bose Electroforce® features. For example, the strain rate could reach

154   very high values in reality due to impact forces, but the characteristics of the material are strain

155   rate dependent [20], and the test speed had to be limited to 3.2%/s so as not to exceed the load

156   cell range and risking rupture. The specimen length also had to be chosen considering the

157   physiologic peak strain (over 100%) and the machine stroke (±6 mm), together with the limited

158   sample extension; these considerations led to the selection of a ~~10~~ 5 mm specimen length. The

159   specimens were clamped by titanium machine grips that were specifically developed for

160   biomaterials and have knurled-flat faces to prevent slipping. The analysis of the video recordings

161   demonstrates that there were neither anomalous behaviours nor failures near the clamps. Sliding

162   through the testing grips was excluded, too, as no abrupt increase or decrease was detected in the

7

163 experimental curves. No marks were observed on the specimen ends, and the extension of the

164 grasped ends was found to be unchanged.

165 Up to the instant preceding the tensile test, all specimens were kept hydrated in physiological

166 solution; no additional hydration was carried out during the test due to the absence of a

167 thermostatic bath. This was not judged to be a major shortcoming because the tests lasted less

168 than one minute. Specimens were constrained to the Bose Electroforce® testing machine,

169 clamping their ends along the longitudinal direction.

170 No preconditioning cycles were performed because the dermal tissue is a bi-phasic structure, like

171 most soft tissues, and preconditioning has been demonstrated to significantly influence the

172 mechanical response of these tissues. Slow viscoelastic phenomena related to fluid flow initiate

173 starting from the very first loading cycles, so the final mechanical properties would depend on the

174 pre-conditioning protocol [21].

175 The testing room temperature was 20° C, while the humidity ranged between 40 and 65%. The

176 displacement was set equal to zero when a 0.05 N force was recorded.

177 Rupture tensile tests were performed for all samples in displacement control at a strain rate of

178 0.032 s^{-1}. The initial gap between the grips was 5 mm.

2.4   Data Elaboration

180 The results of rupture tests on soft tissues are often reported in terms of 'engineering' stress and

181 strain in the literature, with a few exceptions where the specimen section is monitored during

182 tests, and the strain distribution is assessed by full-field techniques [17,22]. In this work, the

183 engineering and true values have been calculated, as detailed in the following.

184 The "engineering curve" is obtained by ignoring the narrowing of the section during the elongation

185 of the sample and referring always to the initial specimen length. The engineering stress σ_e (Eq.

8

186   1) is therefore calculated by dividing the force F by the unloaded-cross sectional area A_0 of the

187   specimen; the engineering strain ε_e (Eq. 2) is expressed as the change in length ΔL per unit of the

188   original length L_0. It should be emphasised that the measurement of the engineering strain would

189   require a dog-bone shaped specimen and a calibrated length whose elongation is monitored, while

190   a rectangular specimen has been here used and its elongation has been evaluated on the basis of

191   the clamp-to-clamp displacement; the authors considered that this was not a hard limitation due

192   to the high compliance of the tissue, which "homogenises" the stress field (see, for example, the

193   work of Taylor et al. on crack propagation [23]). The engineering Young's modulus (E_e) has been

194   calculated from the linear portion of the stress-strain curve [8], which is the so-called 'linear

195   region' where collagen chains are stretched [12,24]: curve data were locally derived with a

196   moving average linear regression, and the constant trend of the derived curve was considered.

197   The true stress σ_t is the ratio between the force and the minimum section A_{min}; it is approximately

198   coincident with the engineering curve, up to the strain where section narrowing becomes

199   conspicuous. The true curve can be obtained by monitoring the neck area during the tensile test:

200   the history of the section variation $A_{min}(t)$ needs to be acquired, monitoring both the specimen

201   width $b_{min}(t)$ and thickness $s_{min}(t)$ at the neck region. In the literature, an alternative expression for

202   the true stress is often used, which relies on the hypothesis of a null variation of the specimen

203   volume [25]: this expression is simpler to be implemented because it requires only the estimation

204   of the real-time specimen length (like for the engineering curve). The respective value σ_{st} will be

205   called the 'simplified true' stress, and it can be obtained from the engineering curve by analytical

206   transformations ($\sigma_{st}= \sigma_e \cdot (1+ \varepsilon_e)$). The corresponding 'simplified true' elastic modulus E_{st} can be

207   calculated on $\sigma_{st}/\varepsilon_e$ curves.

9

208 The evaluation of the true Young's modulus E_t has been performed on the basis of the acquired

209 force and displacement signals and of the specimen shape; given a certain force F, the specimen

210 volume can be divided axially into infinitesimal portions dy whose section is $A(y,F)$. Therefore,

211 the whole specimen elongation Δs_{ab} in the linear portion of the force/displacement curve (a, b,

212 figure 1) can be expressed as

213 $\Delta s_{ab} = \int_{F_a}^{F_b} \int_0^l ds = \int_{F_a}^{F_b} \int_0^l \varepsilon_t \cdot dy = \int_{F_a}^{F_b} \left[\int_0^l \frac{1}{E_t \cdot A(y,F)} dy \right] dF = \frac{1}{E_t} \int_{F_a}^{F_b} \left[\int_0^l \frac{dy}{A(y,F)} \right] dF$

214 where the Young's modulus has been considered to be linear (independent of the force level) and

215 constant all over the specimen, as it should be in the above-mentioned 'linear elastic region'. This

216 formula could not be used up to the failure region (to obtain the true ultimate strain, for example).

217 The 'true' Young's modulus can be so derived:

218 $$E_t = \frac{\int_{F_a}^{F_b} \left[\int_0^l \frac{dy}{A(y,F)} \right] dF}{\Delta s_{ab}}$$

219 The numerator requires the knowledge of the section variation for each force step, and at different

220 quotes (y), and it can be estimated thanks to the photogrammetry set up.

221 A number of descriptive parameters can be so obtained: the ultimate tensile strength (UTS, UTS_t,

222 UTS_{st}), the ultimate deformation ($\varepsilon_{UTS,e}$), and the Young's modulus (E_e, E_{st}, E_t). True values have

223 been calculated only for those decellularization treatments that produced 'engineering' and

224 'simplified true' mechanical properties similar to those of the native dermis (p<0.05, Tukey-

225 Kramer test, as detailed in the following).

2.5 Statistical analysis

227 The mechanical properties of the dermis were reported in relation to the testing direction (CC or

228 ML), the type of decellularization treatment (called NaOH or DMEM in the following), and the

10

229   duration of the treatments (from 0 to 7 weeks at 1 week steps, called T0, T1 …. T7 in the

230   following).

231   The statistical analysis of the experimental results was carried out using a multivariate analysis of

232   variance (Matlab function 'anovan'), followed by a Tukey–Kramer post hoc test, after having

233   tested the normality of the statistical distribution of all parameters by the Lilliefors test function.

234   Significance levels were set to $p < 0.05$ for all tests.

3   Results

236   The analysis of video recordings demonstrated that there were neither anomalous behaviours nor

237   failures near clamps; therefore, all acquired data have been elaborated.

238   Figures 2 shows typical stress/strain curves for the engineering, simplified true and true

239   formulations. Dealing with the ultimate stress (Fig. 3-5), the engineering stress leads to

240   underestimate the UTS by up to -71% and the Young's modulus by up to -84%. The simplified

241   true stress would underestimate the UTS by up to -44%. The error coming from the simplified

242   true stress evaluation demonstrates how the hypothesis that the section variation is inversely

243   proportional to the longitudinal strain (equivalent to the 'constant volume' hypothesis for small

244   deformations) does not hold: this is not surprising because in the literature, both analytical and

245   experimental demonstrations of the soft tissue volume variation during tensile tests can be found

246   [26,27]).

247   All sample properties are shown to be normally distributed, according to the Lilliefors test

248   ($p<0.05$), so the following variance analysis could be performed.

249   The results of the analysis of variance are shown in Table 1: the type of treatment, its duration,

250   and the specimen orientation are all significant factors, as is their interaction ($p<0.05$), with the

11

251   only exception of the specimen orientation for the ultimate strain. The mechanical behaviour

252   along the CC direction is significantly stiffer compared to that in the ML direction, and the

253   mechanical strength is higher (+77.1% E_e, +46.6% UTS_e, -16.1% $\varepsilon_{UTS,e}$, figures 3-5). DMEM

254   treatment is generally less aggressive than NaOH treatment (figures 3-5), and the mechanical

255   properties do not vary monotonously over the treatment length (figures 3-5).

256   A more detailed statistical analysis has been undertaken to establish which factor levels produced

257   significantly different results compared to reference groups (respectively, T0-CC and T0-ML) by

258   means of Tukey-Kramer tests, aiming to identify the best treatment type and duration as the

259   combination producing the results most similar to those of native tissue. Looking at Figures 3-5,

260   only minor differences exist between the engineering and 'simplified true' formulation results,

261   and some general conclusions could be drawn. The tissue properties along the CC direction

262   significantly degrade (lower UTS and E) for all treatments and durations, with $\varepsilon_{UTS,e}$ being the

263   only mechanical property that is not affected significantly. In the ML direction, T0, DMEM T5,

264   DMEM T6, DMEM T7, and NaOH T5 produce similar mechanical properties, according to both

265   the engineering and simplified true formulations. These same treatments have been further

266   investigated to assess if the true stress formulation would lead to the same conclusions. DMEM

267   T5, DMEM T5, NaOH T5, and, partly NaOH T6 (assuming p=0.03) still produced mechanical

268   properties close to those of native tissue for samples cut along the ML direction.

269   Native specimens cut along the CC direction continued to show a higher Young's modulus E_t and

270   UTS_t; no treatment for any duration could preserve these properties.

271   **4   Discussion**

12

272   The native skin from which the HADM scaffold is prepared must be mechanically or physically

273   separated from unwanted tissue and cell structures, and this processing step could alter the

274   integrity and the architecture of the matrix and, in turn, influence the mechanical and material

275   properties of the matrix. The efficiency of cell removal from a tissue is dependent on the origin

276   of the tissue and the specific physical, chemical, and enzymatic methods that are used [28]. A

277   similar consideration holds for the mechanical properties of the scaffold, as demonstrated in this

278   work.

279   Experimental tests were performed at 20 °C, so the measured properties cannot be immediately

280   converted to physiological properties at 37°C. The reason for this choice is the simplification of

281   the experimental set up and being able to compare these results with most works in the literature

282   in which mechanical tests have been carried out at 'room temperature' [8,11,15,29,17,18,30]. The

283   results of the experimental tests were compared, assuming a perfectly uniaxial loading condition

284   and a uniform distribution of collagen fibres. This is a limit in the present experimental set up, as

285   the specimen is rectangular and its contraction is not allowed at the machine clamps, so the

286   uniaxial stress hypothesis is not verified at the specimen ends. Using dog-bone shaped specimens

287   would not completely solve this issue: in the case of longitudinal samples with most collagen

288   fibres oriented axially, it would make no difference because the interrupted fibres (those placed

289   more laterally) would be inactive. Longer specimens would have minimised the influence of the

290   clamped ends, but they would have limited the maximum strain because the employed loading

291   machine allows 12 mm displacement at the most. Finally, it should be stressed that the notch

292   sensitivity in soft tissues is very low [23], so a minor area on the specimen is likely to be affected

293   by the clamps. Ongoing numerical tests are confirming these hypotheses (nonlinear analysis, with

294   large displacements, fig. 6), but the full strain field should be experimentally acquired as a final

13

295   validation. This is a quite demanding experimental set-up. Some authors are setting up systems

296   based on digital image correlation [22]; this is certainly a promising technique that deserves to be

297   considered in future tests on biological tissues.

298   Results have been here expressed through engineering, simplified true and true curves because

299   the results of rupture tests for soft tissues have not always been reported in a standard manner in

300   the literature [18]. Dealing with comparisons among different treatment types and durations and

301   sample directions, all three representations produced substantially similar results.

302   A review of decellularization methods [6] agrees with the results here obtained regarding the

303   NaOH cell removal treatment. In fact, it stated that bases are harsh, so are commonly used to

304   eliminate growth factors from the matrix, even though they decrease ECM mechanical properties

305   more significantly than chemical and enzymatic agents. In this work, the NaOH treatment has

306   been proven to weaken the mechanical properties of the tissue, especially with reference to the

307   cranio-caudal direction. The primary mechanism by which bases such as sodium hydroxide reduce

308   the mechanical properties is the cleavage of collagen fibrils and disruption of collagen crosslinks.

309   Richters *et al.* [31] evaluated a cost-effective method based on low concentrations of NaOH for

310   the decellularization of human donor skin preserved in 85% glycerol, and they found that a 6 week

311   incubation period was optimal, as stated in the present work, while longer periods caused damage

312   to the collagen fibres, although the elastin fibres appeared to be well preserved, and this could

313   explain the different behaviours observed along the cranio-caudal and medio-lateral directions.

314   DMEM coupled to mechanical action has been used as a cell removal treatment for the first time

315   in this work, so similar tests cannot be found in the literature. Other decellularization methods

316   include a wide variety of chemicals, but if the chemicals remain within the tissue in high

317   concentrations after treatment, they can potentially invoke an adverse immune response by the

14

318   host (see, for example, enzymes commonly derived from bovine sources such as DNase, RNase,

319   and trypsin). Herein, one of the most simple decellularization methods was studied (long-term

320   incubation in culture medium), and preliminary immunohistochemical and histological results

321   (unpublished data) demonstrate the complete decellularization of the tissue. DMEM treatment has

322   also proven to be more conservative with reference to the medio-lateral direction because the

323   mechanical properties of specimens treated with DMEM are generally higher than those measured

324   on specimens treated with NaOH for the same number of weeks.

325   From a biological point of view, both DMEM and NaOH show, in the immunohistochemical

326   evaluation, a good decellularization of grafts after only 4 weeks of treatment. However, the

327   DMEM-treated samples exhibit better handling, greater flexibility and lower needle penetration

328   resistance, according to surgeons' evaluations, and are therefore preferable. Additionally, the

329   DMEM treatment avoids the use of chemical agents, as opposed to NaOH, which needs to be

330   neutralized at the end of the decellularization process. Therefore, DMEM is less likely to produce

331   inflammatory responses.

332   The objective of this work was to set up a procedure to perform biomechanical comparisons

333   among decellularization treatments; the complete quantification of the skin's anisotropic

334   behaviour would require a greater number of samples, from different donors, and biaxial testing.

335   This experimental set up can allow only the measurement of the Young's modulus and failure

336   properties along two reference orthogonal directions (parallel and perpendicular to the Langer's

337   lines [8]). Nevertheless, in the following, a comparison with results obtained from other authors

338   [8,32,33] is reported to verify the differences that exist and how they can be justified (Table 2).

339   Nì Annaidh *et al.* [8] reported force–displacement curves for each tensile test performed and

340   calculated the engineering stress and strain. Their standard deviations were much larger; the

15

341 average coefficients of variation (ratios of the standard deviation to the mean) are up to 0.80 for

342 UTS and 0.97 for E, against the values obtained in this work, 0.09 and 0.10, respectively, due to

343 the number of specimens and the specimens having been taken from several donors (Table 2).

344 The values calculated in this work are most similar to those obtained on the 'lower back' and are

345 generally lower (up to -43% for UTS, up to -46% for ε_{UTS}, up to -68% for E) compared to those

346 reported in [8]. This can be explained by the smaller size of the specimens, which results in more

347 severe striction and consequently lower nominal stresses.

348 Yoder and Elliott [32] characterized human allografts by considering the engineering stress and

349 calculated two-dimensional Langrangian strains from optical images using Vic2D software. The

350 Young's modulus (Table 2) compares favourably to the results here reported for DMEM and

351 NaOH at T5 or T6 for engineering curves with reference to the ML direction. A 20 times higher

352 E along the 'parallel' direction is reported in [32]; this result is against the findings of this work

353 and [8], which both report a lower level of anisotropy in tested tissues.

354 Up to now, the failure properties and the elastic behaviour for static loads has been investigated,

355 as critical aspects of dermal patches include stiffness mismatch [35] and the eventual failure.

356 Nevertheless, cyclic loading parameters also need to be considered because in a highly

357 collagenous tissue such as skin, the elastic recoil and hysteresis of the material would be of utmost

358 importance.

References

360

361 [1] Sander EA, Lynch KA, Boyce ST. Development of the mechanical properties of engineered
362   skin substitutes after grafting to full-thickness wounds. J Biomech Eng 2014;136:051008.
363   doi:10.1115/1.4026290.
364

16

365 [2]   Sun BK, Siprashvili Z, Khavari PA. Advances in skin grafting and treatment of cutaneous
366   wounds. Science 2014;346:941–5. doi:10.1126/science.1253836.
367

368 [3]   Wong DJ, Chang HY. Skin tissue engineering. Harvard Stem Cell Institute; 2009.
369

370 [4]   Badylak SF, Freytes DO, Gilbert TW. Reprint of: Extracellular matrix as a biological
371   scaffold material: Structure and function. Acta Biomater 2015;23:S17–26.
372   doi:10.1016/j.actbio.2015.07.016.
373

374 [5]   Deeken CR, Eliason BJ, Pichert MD, Grant SA, Frisella MM, Matthews BD.
375   Differentiation of biologic scaffold materials through physicomechanical, thermal, and
376   enzymatic degradation techniques. Ann Surg 2012;255:595–604.
377   doi:10.1097/SLA.0b013e3182445341.
378

379 [6]   Crapo PM, Gilbert TW, Badylak SF. An overview of tissue and whole organ
380   decellularization processes. Biomaterials 2011;32:3233–43.
381   doi:10.1016/j.biomaterials.2011.01.057.
382

383 [7]   Butler DL, Goldstein SA, Guilak F. Functional tissue engineering: the role of
384   biomechanics. J Biomech Eng 2000;122:570–5.
385

386 [8]   Ní Annaidh A, Bruyère K, Destrade M, Gilchrist MD, Otténio M. Characterization of the
387   anisotropic mechanical properties of excised human skin. J Mech Behav Biomed Mater
388   2012;5:139–48. doi:10.1016/j.jmbbm.2011.08.016.
389

390 [9]   Moore MA, Samsell B, Wallis G, Triplett S, Chen S, Jones AL, et al. Decellularization of
391   human dermis using non-denaturing anionic detergent and endonuclease: a review. Cell
392   Tissue Bank 2015;16:249–59. doi:10.1007/s10561-014-9467-4.
393

394 [10] Eshel H, Lanir Y. Effects of strain level and proteoglycan depletion on preconditioning and
395   viscoelastic responses of rat dorsal skin. Ann Biomed Eng 2001;29:164–72.
396

397 [11] Sanders R. Torsional elasticity of human skin in vivo. Pflugers Arch 1973;342:255–60.
398

399 [12] Fung YC. Biomechanics - Mechanical Properties of Living Tissues | Y. C. Fung | Springer.
400   2nd ed. New York: Springer-Verlag; 1993.
401

402 [13] Pereira BP, Lucas PW, Swee-Hin T. Ranking the fracture toughness of thin mammalian

17

403   soft tissues using the scissors cutting test. J Biomech 1997;30:91–4.
404

405   [14] Del Prete Z, Antoniucci S, Hoffman AH, Grigg P. Viscoelastic properties of skin in Mov-
406   13 and Tsk mice. J Biomech 2004;37:1491–7. doi:10.1016/j.jbiomech.2004.01.015.
407

408   [15] Muñoz MJ, Bea J a., Rodríguez JF, Ochoa I, Grasa J, Pérez del Palomar a., et al. An
409   experimental study of the mouse skin behaviour: Damage and inelastic aspects. J Biomech
410   2008;41:93–9. doi:10.1016/j.jbiomech.2007.07.013.
411

412   [16] Liu Z, Yeung K. On Preconditioning and Stress Relaxation Behaviour of Fresh Swine Skin
413   in Different Fibre Direction. Biomed Pharm Eng 2006 ICBPE 2006 Int Conf 2006:221–6.
414

415   [17] Jacquemoud C, Bruyere-Garnier K, Coret M. Methodology to determine failure
416   characteristics of planar soft tissues using a dynamic tensile test. J Biomech 2007;40:468–
417   75. doi:10.1016/j.jbiomech.2005.12.010.
418

419   [18] Khanafer K, Schlicht MS, Berguer R. How Should We Measure and Report Elasticity in
420   Aortic Tissue? Eur J Vasc Endovasc Surg 2013;45:332–9. doi:10.1016/j.ejvs.2012.12.015.
421

422   [19] Euro Tissue Bank - Manual n.d. http://www.eurotissuebank.nl/euro-skin-bank-huidbank-
423   esb-en-GB/what-is-donor-skin/manual/ (accessed October 14, 2015).
424

425   [20] Arumugam V, Naresh MD, Sanjeevi R. Effect of strain rate on the fracture behaviour of
426   skin. J Biosci 1994;19:307–13. doi:10.1007/BF02716820.
427

428   [21] Hosseini SM, Wilson W, Ito K, van Donkelaar CC. How preconditioning affects the
429   measurement of poro-viscoelastic mechanical properties in biological tissues. Biomech
430   Model Mechanobiol 2013:503–13. doi:10.1007/s10237-013-0511-2.
431

432   [22] Bel-Brunon A, Kehl S, Martin C, Uhlig S, Wall WA. Numerical identification method for
433   the non-linear viscoelastic compressible behavior of soft tissue using uniaxial tensile tests
434   and image registration - application to rat lung parenchyma. J Mech Behav Biomed Mater
435   2014;29:360–74. doi:10.1016/j.jmbbm.2013.09.018.
436

437   [23] Taylor D, O'Mara N, Ryan E, Takaza M, Simms C. The fracture toughness of soft tissues.
438   J Mech Behav Biomed Mater 2012;6:139–47. doi:10.1016/j.jmbbm.2011.09.018.
439

440   [24] Özkaya N, Nordin M, Goldsheyder D, Leger D. Fundamentals of Biomechanics -

18

441 Equilibrium, Motion, and | Nihat Özkaya | Springer. 3rd ed. New York: Springer-Verlag;
442 2012.
443

444 [25] Silver FH, Freeman JW, DeVore D. Viscoelastic properties of human skin and processed
445   dermis. Skin Res Technol 2001;7:18–23.
446

447 [26] Adeeb S, Ali A, Shrive N, Frank C, Smith D. Modelling the Behaviour of Ligaments: A
448   Technical Note. Comput Methods Biomech Biomed Engin 2004;7:33–42.
449   doi:10.1080/10255840310001637266.
450

451 [27] Reese SP, Maas SA, Weiss JA. Micromechanical models of helical superstructures in
452   ligament and tendon fibers predict large Poisson's ratios. J Biomech 2010;43:1394–400.
453   doi:10.1016/j.jbiomech.2010.01.004.
454

455 [28] Chen R-N, Ho H-O, Tsai Y-T, Sheu M-T. Process development of an acellular dermal
456   matrix (ADM) for biomedical applications. Biomaterials 2004;25:2679–86.
457   doi:10.1016/j.biomaterials.2003.09.070.
458

459 [29] Li L, Qian X, Wang H, Hua L, Zhang H, Liu Z. Power type strain energy function model
460   and prediction of the anisotropic mechanical properties of skin using uniaxial extension
461   data. Med Biol Eng Comput 2013;51:1147–56. doi:10.1007/s11517-013-1098-6.
462

463 [30] Ní Annaidh A, Bruyère K, Destrade M, Gilchrist MD, Maurini C, Otténio M, et al.
464   Automated Estimation of Collagen Fibre Dispersion in the Dermis and its Contribution to
465   the Anisotropic Behaviour of Skin. Ann Biomed Eng 2012;40:1666–78.
466   doi:10.1007/s10439-012-0542-3.
467

468 [31] Richters CD, Pirayesh A, Hoeksema H, Kamperdijk EWA, Kreis RW, Dutrieux RP, et al.
469   Development of a dermal matrix from glycerol preserved allogeneic skin. Cell Tissue Bank
470   2008;9:309–15. doi:10.1007/s10561-008-9073-4.
471

472 [32] Yoder JH, Elliott DM. Nonlinear and anisotropic tensile properties of graft materials used
473   in soft tissue applications. Clin Biomech 2010;25:378–82.
474   doi:10.1016/j.clinbiomech.2010.01.004.
475

476 [33] Edwards C, Marks R. Evaluation of biomechanical properties of human skin. Clin
477   Dermatol 1995;13:375–80. doi:10.1016/0738-081X(95)00078-T.
478

479 [34] Daly CH. Biomechanical properties of dermis. J Invest Dermatol 1982;79 Suppl 1:17s –
      19

480   20s.
481

482   [35]   Hopp I, Michelmore A, Smith LE, Robinson DE, Bachhuka A, Mierczynska A, et al. The
483   influence of substrate stiffness gradients on primary human dermal fibroblasts.
484   Biomaterials 2013;34:5070–7. doi:10.1016/j.biomaterials.2013.03.075.
485

486

487

488

489 *Table 1: Anova results for the ultimate stress, ultimate strain and elastic modulus with reference to*
490 *the engineering formulation. Boldface characters are used to highlight factors that are not significant*
491 *(p > 0.05)."*
492

Ultimate Stress

Source	Sum Sq.	DOF	Mean Sq.	F	p
Treatment	30.90	1	30.90	128.22	6.28E-17
Orientation	11.00	1	11.00	45.67	4.94E-09
Duration	257.24	7	36.75	152.50	2.08E-37
Treatment*Orientation	12.04	1	12.04	49.97	1.41E-09
Treatment*Duration	13.57	7	1.94	8.05	5.45E-07
Orientation*Duration	64.42	7	9.20	38.19	1.67E-20
Error	15.42	64	0.24		
Total	421.99	95			

Ultimate Strain

Source	Sum Sq.	DOF	Mean Sq.	F	p
Treatment	0.37	1	0.37	40.22	2.61E-08
Orientation	0.00	1	0.00	0.27	**6.05E-01**
Duration	0.45	7	0.07	7.00	3.42E-06
Treatment*Orientation	0.06	1	0.06	6.73	1.17E-02
Treatment*Duration	0.76	7	0.11	11.80	1.52E-09
Orientation*Duration	0.44	7	0.06	6.86	4.40E-06
Error	0.59	64	0.01		
Total	2.94	95			

Elastic Modulus

21

Dermis Mechanical Behaviour after Different Cell Removal Treatments

Source	Sum Sq.	DOF	Mean Sq.	F	p
Treatment	318.03	1	318.03	108.72	1.98E-15
Orientation	98.80	1	98.80	33.77	2.13E-07
Duration	748.22	7	106.89	36.54	5.10E-20
Treatment*Orientation	44.72	1	44.72	15.29	2.25E-04
Treatment*Duration	295.62	7	42.23	14.44	4.16E-11
Orientation*Duration	578.59	7	82.66	28.26	2.67E-17
Error	187.22	64	2.93		
Total	2386.48	95			

493
494

495

496

22

497

498

499 *Table 2 Mechanical properties of skin in literature and in this work (average± SD).*

Author	Skin Location (Langer Line Orientation)	UTS (MPa)	Failure Stretch	Elastic Modulus (MPa)	Reference Variables
Nì Annaidh *et al.* [8]	Middle Back (Parallel)	28.64 ± 9.03	1.46 ± 0.07	112.47 ± 36	σ_e, ε_e
	Bottom Back (Parallel)	17.60 ± 4.77	1.74 ± 0.32	73.81 ± 19.41	
	Middle Back (Perpendicular)	16.53 ± 5.71	1.52 ± 0.08	63.75 ± 24.59	
	Bottom Back (Perpendicular)	10.56 ± 8.41	1.61 ± 0.14	37.66 ± 36.41	
Edwards C. [33]		5-30	35-115%	15-150	Various authors
Yoder and Elliott [32]	Alloderm (Parallel)			221.48 ± 141.20	$\sigma_e, \varepsilon_{Lagrange}$
	Alloderm (Perpendicular)			11.21 ± 3.53	
This work (T_0)	Back (craniocaudal)	10.28 ± 0.96	0.77 ± 0.08	13.01 ± 2.61	$\sigma_e, \varepsilon_e, E_e$
		18.38 ± 2.42			σ_{st}
		33.95 ± 4.93		43.63 ± 6.29	σ_t, E_t
	Back (medio-lateral)	7.01 ± 0.10	0.93 ± 0.15	7.20 ± 1.22	$\sigma_e, \varepsilon_e, E_e$
		13.81 ± 2.80			σ_{st}
		24.11 ± 3.24		29.77 ± 7.54	σ_t, E_t

500

23

501   **Figure Captions**

502

503   **Figure 1.** (Left) An interpolated engineering stress-strain curve, its descriptive parameters, and

504   specimen images. (Right) Experimental stress strain curves, where point 'U' represents the

505   average ultimate strain/stress point with its standard deviations; a) DMEM, T6, ML direction; b)

506   DMEM, T6, CC direction; c) NaOH, T6, ML direction; d) NaOH, T6, CC direction.

507   **Figure 2.** Engineering, simplified true, and true formulation curves; a) DMEM, T6, ML direction;

508   b) DMEM, T6, CC direction; c) NaOH, T6, ML direction; d) NaOH, T6, CC direction"

509   **Figure 3.** UTS values obtained from engineering, simplified true, and true formulations for

510   different decellularization treatments. Left side (grey background): results obtained along CC

511   direction; right side (white background): results obtained along ML direction

512   **Figure 4**. Engineering strain corresponding to the ultimate stress for different decellularization

513   treatments. Left side (grey background): results obtained along CC direction; right side (white

514   background): results obtained along ML direction

515   **Figure 5.** Elastic modulus values for different decellularization treatments. Left side (grey

516   background): results obtained along CC direction; right side (white background): results obtained

517   along ML direction

518   **Figure 6.** Axial stress distribution from finite element analysis: nonlinear 3D analysis (Ansys

519   Mechanical APDL); hexahedral mesh of 600 elements (SOLID186); E=14 MPa; Poisson's ratio

520   = 0.4; all displacements have been constrained at the lower edge, while the upper edge can only

521   move vertically, where u=2 mm (ε=0.4) has been applied

522

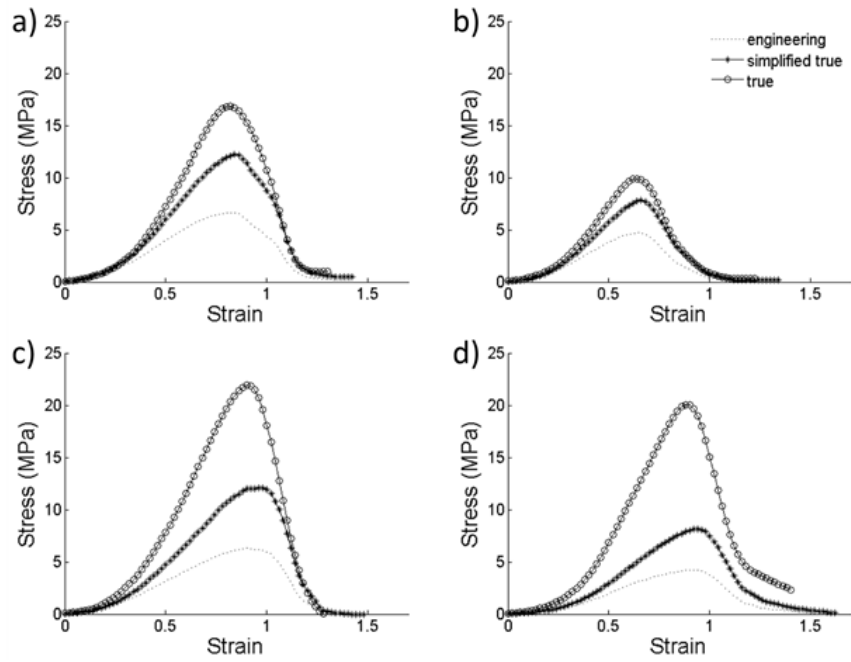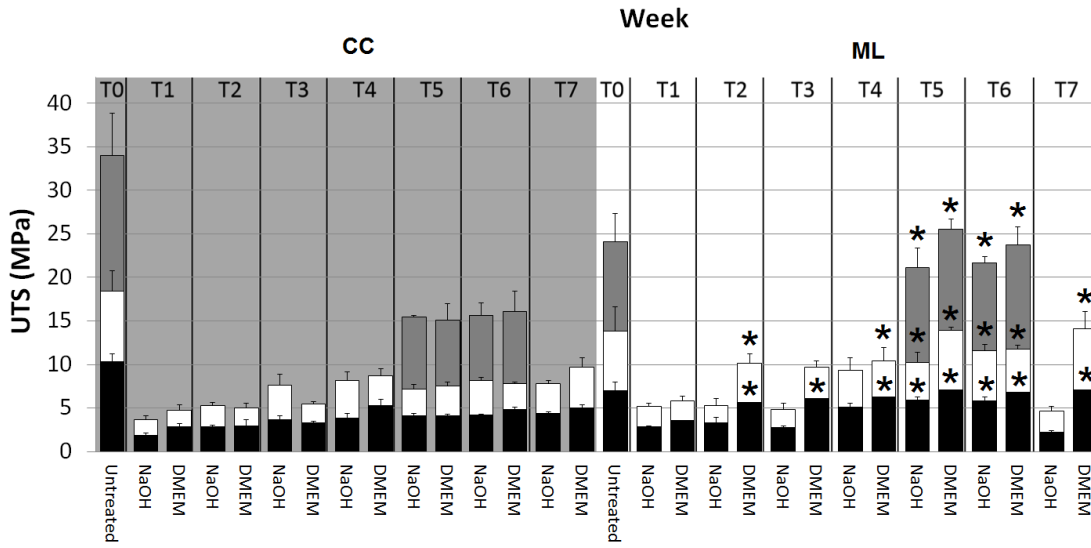24

523   **Figure 1**
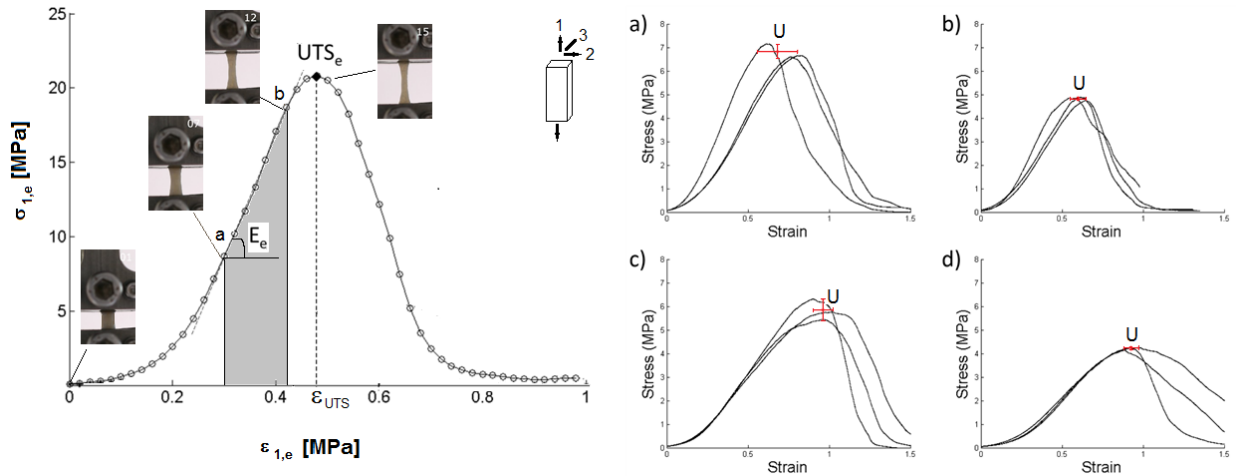
524
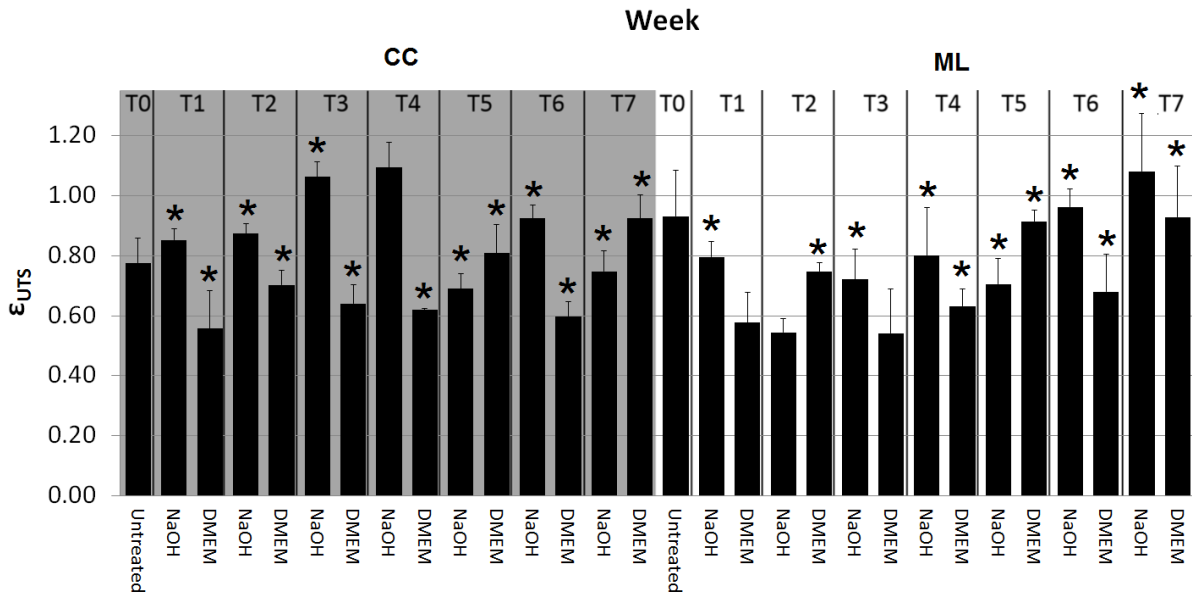
525   **Figure 2**

526

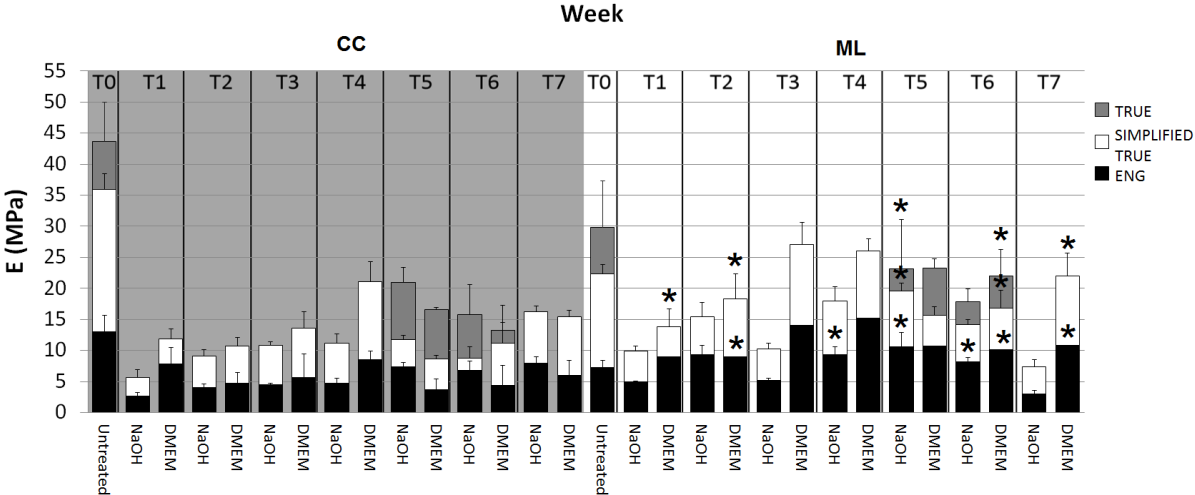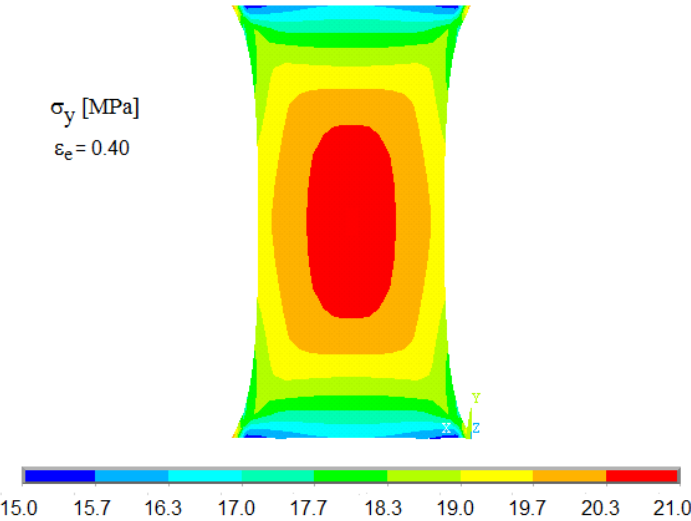527

528 **Figure 3**

529

530 **Figure 4**

531

532

533   **Figure 5**

534

535   **Figure 6**

536

27